Upstream-downstream asymmetry in multiscale interaction underlying the Northern Hemisphere atmospheric blockings

Jiwang Ma,[a,b] X. San Liang,[a,b,c]

[a] *Department of Atmospheric and Oceanic Sciences, Fudan University, Shanghai, China*

[b] *The Artificial Intelligence Group, Division of Frontier Research, Southern Marine Science and Engineering Guangdong Laboratory (Zhuhai), Zhuhai, China*

[c] *IRDR ICoE on Risk Interconnectivity and Governance on Weather/Climate Extremes Impact and Public Health, Fudan University, Shanghai, China*

Corresponding author: X. San Liang, sanliang@courant.nyu.edu

ABSTRACT

The typical blockings over the Pacific, Atlantic, and Ural Mountain regions are investigated for an understanding of their dynamical interactions in a unified treatment with their respective basic flows and high-frequency processes, respectively. Thanks to the localized nature of the new methodology as used in this study, for the first time we identify a dipolar structure (for each of the three regions) in the map of the interscale energy transfer from the basic flow to the composite blocking, with a positive center upstream and a negative center downstream. This indicates the crucial role of the instability of the basic flow in the maintenance of blockings, which has been overlooked due to the bulk nature of the spatially integrated energetics (by summing the transfer over the whole blocking, the two centers essentially cancel out, leaving an insignificant bulk transfer). For the interaction between the blocking and the high-frequency storms, the well-known critical role of the upscale forcing in blocking development is confirmed. But, unexpectedly, except for that over the Atlantic where the forcing exists throughout, over the other two regions the forcing is found to occur mainly in downstream. This is quite different from what the classical theory, e.g., the famous eddy strain mechanism of Shutts (1983), would predict.

1. Introduction

File generated with AMS Word template 2.0

Early Online Release: This preliminary version has been accepted for publication in *Journal of the Atmospheric Sciences*, may be fully cited, and has been assigned DOI 10.1175/JAS-D-22-0220.1. The final typeset copyedited article will replace the EOR at the above DOI when it is published.

Atmospheric blocking is a quasi-stationary high pressure system which persists for a duration longer than the typical synoptic waves, exerting significant influence on the ambient weather and climate. Particularly, it is found to have close relationship to extreme events---heatwave, cold air break, drought, flood, etc., which are of great societal concern (e.g., Trigo et al. 2004; Hong et al. 2011; Dole et al. 2011; Dong et al. 2018; Fang and Lu 2020; Kautz et al. 2022).

Previous studies have shown that multiscale interactions between scales are essential to the blocking dynamics. Particularly, the critical role of upscale forcing from high-frequency (small scales) to low frequency processes (or mean flow) have been emphasized from different perspectives (e.g., Austin 1980; Illari and Marshall 1983; Tsou and Smith 1990; Robinson, 1991; Luo et al. 2014, 2019; Fournier 2003; Hansen and Chen 1982; Ma and Liang 2017; Nakamura and Huang 2018; Tanaka 1990; Martineau et al. 2022; Nakamura and Wallace 1993; Nakamura et al. 1997; Miller and Wang 2022), including momentum flux, head flux, potential vorticity, geopotential height, wave activity, energetics, etc. In this study, we will focus on the perspective of multiscale energetics. Roughly, the multiscale blocking energetics studies could be classified into three categories --- global, partially local, and fully local energetics. Global or nonlocal energetics studies are generally based on Reynolds mean (e.g., Holopainen and Fortelius 1987) or Fourier spectral analysis (e.g., Hansen and Chen 1982); partially local analysis employs wavelet analysis as the research tool and is pioneered by Fournier (2002, 2003); fully local analysis is conducted by Ma and Liang (2017), where multiscale window transform (MWT, Liang and Anderson, 2007), theory of canonical transfer (Liang 2016), and the MWT-based multiscale energetics analysis (Liang and Robinson 2005, 2007; Liang 2016) are utilized to fulfill the task (refer to Section 2 for details). The fully local multiscale energetics analysis is advantageous for understanding the blocking dynamics in that it produces spatiotemporal field-like energetic terms, i.e., four-dimensional fields of energetics, allowing one to check, at the finest resolution, the multiscale interactive information at every spatial location and each time point. Though the fully local multiscale energetics analysis for the wintertime Atlantic blockings has been studied by Ma and Liang (2017), this analysis has not been conducted for the blockings over other regions. As previous studies have demonstrated that the multiscale blocking processes over different regions may differ (e.g., Nakamura et al. 1997; Drouard and Woollings 2018; Miller and Wang 2022; Martineau et al. 2022), we are therefore expecting to unravel different dynamics underlying the other blockings. This paper is organized as follows: The datasets and methods

Accepted for publication in *Journal of the Atmospheric Sciences*. DOI 10.1175/JAS-D-22-0220.1.

are described in Section 2. Reconstructed blocking signals are given in Section 3. The corresponding multiscale interactive processes are analyzed in Sections 4. Section 5 concludes the study and offers a discussion of some remaining issues.

2. Data and methods

a. Data

This study is based on the ERA-40 (https://apps.ecmwf.int/datasets/data/era40-daily/levtype=pl/) dataset from the European Centre for Medium-Range Weather Forecasts (ECMWF)(Uppala et al. 2005), which includes temperature (T), wind components (u, v, ω), and geopotential (Φ). In this study, we choose a time resolution of 6 h and a spatial resolution of $2.5^{\circ} \times 2.5^{\circ}$. The spatial domain covers the zonal circle between 30° and $85^{\circ}\mathrm{N}$, with 15 standard *p* levels from 1000 to 50 hPa. As will be mentioned below, the number of the time steps should be arranged to be a power of 2. We hence choose a period starting September 1, 1957 and ending May 21, 2002, which results in series with 2^{16} time steps.

b. Multiscale window transform, multiscale energetics analysis, and canonical transfer

1) MULTISCALE WINDOW TRANSFORM

Multiscale window transform (MWT) is a functional analysis apparatus originally developed for the very purpose of energetics studies (Liang and Anderson, 2007). While orthogonally decomposing a field by scales and providing filtered fields (reconstructions) on different scales, it also provides transform coefficients for the corresponding filtered fields. This not only ensures energy conservation during a decomposition (thanks to the Parseval relation in functional analysis), but also makes it possible to express multiscale energies in terms of transform coefficients. This is in contrast to most of the widely used filters, which do not have transform coefficients and hence actually cannot have this multiscale energy representation. (It is a common practice to use the square of filtered fields as multiscale energy, but that is conceptually wrong---think about the energy in Fourier space when examining a power spectrum.)

With MWT a field can be reconstructed onto some range of scales, or *scale windows* as called. In this study we will need a low-frequency window, a blocking scale window (or simply blocking window), and a high-frequency window. For convenience, we will denote these windows as 0, 1, 2, respectively. More comprehensive introduction of MWT is beyond

File generated with AMS Word template 2.0

Accepted for publication in *Journal of the Atmospheric Sciences*. DOI 10.1175/JAS-D-22-0220.1.

this study; readers are referred to Liang and Anderson (2007) for details (there is a more readable introduction in Liang 2016). Here we simply write the MWT of a field, say u , as $\hat{u}_n^{\sim\varpi}$, where n is the time step, $\varpi = 0{,}1{,}2$ denotes the scale window. The corresponding reconstructions, i.e., filtered fields, are written as $u^{\sim\varpi}$. For easy reference, the following is a very brief introduction.

Given a time series $u(t)$, for a three-scale window decomposition, u can be reconstructed onto three windows:

$$u(t) = \sum_{\varpi=0}^{2} u^{\varpi}(t), \tag{1}$$

with the notations $\varpi = 0$, 1 and 2 respectively signifying the basic flow window, blocking window, and high-frequency window. $u^{\sim\varpi}(t)$ is the reconstruction of u on window ϖ, which can be understood as the filtered fields on that window. Formally, it is

$$u^{\varpi}(t) = \sum_{n=0}^{2^{j_2}-1} \hat{u}_n^{\varpi} \phi_n^{j_2}(t), \tag{2}$$

where

$$\hat{u}_n^{\varpi} = \int_0^1 u^{\varpi}(t) \phi_n^{j_2}(t)\, dt, \tag{3}$$

and $\phi(t)$ is a localized scaling basis, j is the wavelet scale level and n is the discrete time step in the sampling space. Eqns. (2) and (3) make a transform-reconstruction pair; they are the multiscale window reconstruction (MWR) and its peer, MWT, respectively. For each MWR of a time series $u(t)$, $u^{\sim\varpi}(t)$, there is a corresponding transform coefficient, denoted as $\hat{u}_n^{\sim\varpi}$. Note $\hat{u}_n^{\sim\varpi}$ is constant in t, in contrast to $u^{\sim\varpi}(t)$, the reconstructed or filtered field. The time dependence of $\hat{u}_n^{\sim\varpi}$ is revealed in the discrete time step n. The *time-dependent* energy on window ϖ proves to be the square of the transform coefficients, i.e., $(\hat{u}_n^{\sim\varpi})^2$, multiplied by some constant factor (cf. Liang and Anderson 2007). Note that it is by no means the trivial square of the filtered field, i.e., $\left[u^{\varpi}(t)\right]^2$, as commonly used in the literature.

2) CANONICAL TRANSFER

Accepted for publication in *Journal of the Atmospheric Sciences*. DOI 10.1175/JAS-D-22-0220.1.

Ever since Lorenz's seminal work (1955), multiscale energetics analysis has become a powerful tool to diagnose the dynamical processes underlying atmospheric phenomena. As is well known, Lorenz's formalism is in an integral/average form, lacking the needed local information for most of the weather and climate processes, particularly for those developing processes which may also be on the move. A lot of studies attempt to get around this difficulty by simply removing the average operators. This simple practice seems to be effective, but, unfortunately, is conceptually incorrect. As elaborated in Liang (2016) and many other publications (a most recent one is Yang et al., 2020), that removing the average operator from the eddy energy formula with a Reynolds decomposition does not yield the "localized eddy energy". In fact, it is not at all energy in the physical sense. The average operator allows for a connection of the so-obtained eddy energy to the eddy energy in the Fourier space through the renowned Parseval relation in functional analysis; otherwise the so-obtained "energy" would not be conserved. Second, localizing the bulk Lorenz formalism is faced with an obstacle on how to separate the cross-scale transfer from in-scale transport, which is rather subjective in classical formalisms and not unique. This is a rather fundamental problem (as identified in some early pioneering studies such as Plumb 1983) which, however, has been mostly overlooked. Liang and Robinson (2005, 2007) are the first to tackle this systematically, using the aforementioned MWT as the machinery. The thus-obtained transfer has been termed as *canonical transfer*. In the following we simply write out the formula for computation; the reader is referred to Liang (2016) for details.

As derived in Liang (2016), the multiscale kinetic energy (KE) and available potential energy (APE) equations are (for simplicity, the subscript *n* has been suppressed in the transform notations):

$$\frac{\partial K^{\varpi}}{\partial t} + \underbrace{\nabla \cdot \left[\frac{1}{2}\widehat{(\mathbf{v}\mathbf{v}_h)}^{\sim\varpi} \cdot \hat{\mathbf{v}}_h^{\sim\varpi}\right]}_{\nabla\cdot\mathbf{Q}_K^{\varpi}} =$$

$$\underbrace{\frac{1}{2}\left\{\widehat{(\mathbf{v}\mathbf{v}_h)}^{\sim\varpi} : \nabla\hat{\mathbf{v}}_h^{\sim\varpi} - \left[\nabla \cdot \widehat{(\mathbf{v}\mathbf{v}_h)}^{\sim\varpi}\right] \cdot \hat{\mathbf{v}}_h^{\sim\varpi}\right\}}_{\Gamma_K^{\varpi}} - \underbrace{\nabla \cdot \left(\hat{\mathbf{v}}^{\sim\varpi}\hat{\Phi}^{\sim\varpi}\right)}_{\nabla\cdot\mathbf{Q}_P^{\varpi}} - \underbrace{\hat{\omega}^{\sim\varpi}\hat{\alpha}^{\sim\varpi}}_{b^{\varpi}} + F_K^{\varpi} \qquad (4)$$

$$\frac{\partial A^{\varpi}}{\partial t} + \underbrace{\nabla \cdot \left[\frac{1}{2}c\widehat{(\boldsymbol{v}T)}^{\sim\varpi}\hat{T}^{\sim\varpi}\right]}_{\nabla\cdot\boldsymbol{Q}_A^{\varpi}} =$$

File generated with AMS Word template 2.0

Accepted for publication in *Journal of the Atmospheric Sciences*. DOI 10.1175/JAS-D-22-0220.1.

$$\underbrace{\frac{c}{2}\left[\widehat{(\boldsymbol{v}T)}^{\sim\varpi}\cdot\nabla\hat{T}^{\sim\varpi}-\hat{T}^{\sim\varpi}\nabla\cdot\widehat{(\boldsymbol{v}T)}^{\sim\varpi}\right]}_{\Gamma_A^{\varpi}}+\underbrace{\widehat{\omega}^{\sim\varpi}\hat{\alpha}^{\sim\varpi}}_{b^{\varpi}}+F_A^{\varpi} \quad (5)$$

where K^{ϖ} and A^{ϖ} are the KE and APE on window ϖ , $\mathbf{v}_h$ is the horizontal component of velocity, ω vertical velocity, Φ geopotential, T temperature, and α is the specific volume. The symbol " $\widehat{\ }^{\sim\varpi}$" means the MWT transform coefficient on scale window ϖ. Note here there should be a subscript *n* indicating the time step, but for clarity it has been suppressed. The operator ":" in Eq. (4) is defined as (AB):(CD) = (A· C)(B· D). Other symbols are conventional. The terms $\nabla\cdot Q_K$, $\nabla\cdot Q_P$, Γ_K, b and F_K are KE transport, pressure work, KE canonical transfer among scales, buoyancy conversion and dissipation, respectively. This transfer Γ has a nice property $\sum_{\varpi}\sum_n \Gamma_n^{\varpi}$=0, which means that this kind of process only redistributes energy among scales. It does not generate nor destroy energy as a whole. In other words, it ensures energy conservation, in contrast to its traditional counterparts. In terms of canonical transfer, the fully localized multiscale interactions underlying a blocking hence can be quantitatively investigated.

MWT and the MWT-based multiscale energetics analysis have been validated with benchmark geophysical fluid dynamical processes (e.g., Liang and Robinson, 2007), and applied with success in many real atmosphere-ocean-climate problems. The most recent ones include those on storm track (Zhao et al. 2019), atmospheric blocking (Ma and Liang 2017), cold wave outbreak (Xu and Liang 2020), squall line (Guo and Liang 2022), tropical cyclone (Song et al. 2022); Gulf of Mexico circulation (Yang et al. 2020, 2021), to name a few.

c. Blocking index

We use for the purpose of this study the blocking index as proposed by Lejenäs and Økland (1983) and modified by Tibaldi and Molteni (1990) (called TM index herein). We use it to pick up blocking episodes during the whole range of the period based on a criterion, with two quantities:

$$\mathrm{GHGS}=\frac{Z(\phi_0)-Z(\phi_s)}{\phi_0-\phi_s}\ \text{and,}$$

$$\mathrm{GHGN}=\frac{Z(\phi_n)-Z(\phi_0)}{\phi_n-\phi_0},$$

where GHGS and GHGN represent the southern and northern parts of the 500-hPa geopotential height (Z) gradient, respectively, and ϕ denotes latitude and $\phi_n=80+\Delta$, $\phi_0=$

Accepted for publication in *Journal of the Atmospheric Sciences*. DOI 10.1175/JAS-D-22-0220.1.

$60 + \Delta$, $\phi_s = 40 + \Delta$, while Δ is a parameter with a value of -5, 0, or 5. If the following conditions are satisfied for at least one of the Δ values at one longitude, then the circulation at this longitude is regarded as blocking,

$$\text{GHGS} > 0,$$

$$\text{GHGN} < -10\text{m/deg}.$$

Blocking processes usually have relatively large spatial scales and last for a relatively long time. To make sure the blocking events we gain here are consistent with these facts, only those meeting the TM index criterion at a longitudinal range of 12.5 or more and a temporal duration of more than 4 days are admitted for the composition, as suggested by Barriopedro et al. (2006) and Pelly and Hoskins (2003). The strength of a blocking is determined by the difference of GHGS and GSGN. For an event, the day when the strength gets its maximum is defined as blocking day 0, or simply day 0. The days before and after that day are accordingly days …-3, -2, -1 and 1, 2, 3…, respectively. The composition of blocking events is achieved by averaging the variables on the same blocking day.

d. Regions selection

By our experience the multiscale energy transfers underlying the blockings over different regions may vary a lot. It is impossible to discuss all the features as identified in just one study. We hence select three typical regions, i.e. the Atlantic-Europe, Eastern Pacific and Ural Mountain regions, for the purpose of this study. The first two regions are selected because they are the two most frequented regions along the North Hemisphere zonal circle, as identified in many studies (e.g., Barnes et al. 2011; Martineau et al. 2022). They are also regions of maximum frequency of the so-called “persistent anomalies” episodes, which are closely related to blockings and extreme events, as demonstrated by Dole and Gordon (1983) and Miller et al. (2020). Another such region has been identified near the Ural Mountain (Dole and Gordon, 1983; Miller et al., 2020), which, though, has its distinct frequency of occurrence of blocking events. For these reasons, these three regions, i.e., the Pacific, Atlantic and Ural Mountain regions, are selected. According to the criteria mentioned in the preceding subsection, 172, 362, and 141 blocking events are respectively selected for these regions.

e. Scale separation and blocking geopotential reconstruction

Accepted for publication in *Journal of the Atmospheric Sciences*. DOI 10.1175/JAS-D-22-0220.1.

Sawyer (1970) demonstrates that blockings are closely related to the 15-60 day low-frequency signals. Based on this fact, we separate the original fields into three parts on three scale windows, i.e., the basic-flow window (longer than 64 days), blocking window (16-64 days) and high-frequency window (less than 16 days), using MWT as introduced in Section 2b. (To test the sensitivity of the outcomes to window bounds, we have also tried another pair of bounds, i.e., 8 days and 32 days, for the blocking window. That is to say, the upper bound is now changed from 64 days to 32 days, and the lower bound is reduced from 16 days by half to 8 days. The outcomes are found insensitive to this window bounds change.) Following the procedures in Section 2c, we composite the geopotential and KE on the blocking window and on day 0 over the three regions. The result is shown in Fig. 1. A clear high cell is depicted over all the three regions. Another prominent feature is that there is a low anomaly located at the south of the high cell, which is believed to play a significant role in the cold event in previous studies (e.g., Luo et al. 2021). Actually, these two cells are dynamically a whole, as will be clear in the next section. The blocking signals we get here are consistent with previous studies (e.g., Luo et al. 2016; Ma and Liang 2017). As a result, we can safely conclude that the scale separation and composition scheme used here are reasonable and suitable for the purpose of this study. By checking the KE anomaly, it is clear that the KE is concentrated more at the eastern half of blocking for all the three regions, consistent with Ma and Liang (2017). As we will show in the next section, the eastern half (or the downstream) of the blocking is exactly where the upscale forcing prefers.

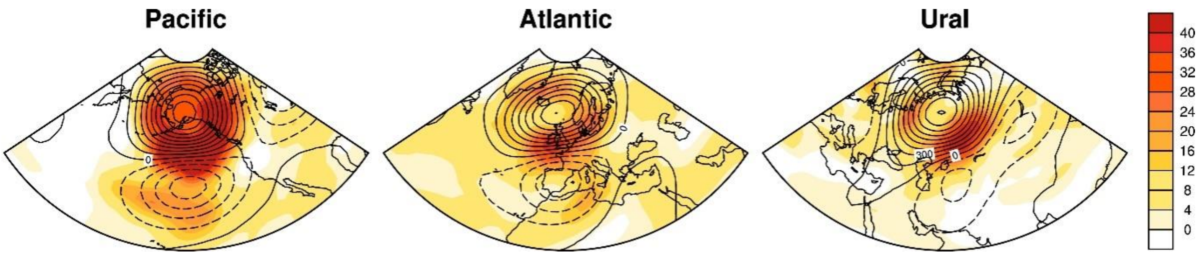

Fig. 1. Reconstructed geopotential (contoured, in m^2/s^2) and KE anomaly relative to its climatology (shaded, in m^2/s^2) on the blocking window over the Pacific, Atlantic and Ural on day 0 at 300 hPa.

3. Multiscale interactions underlying blocking

Hansen and Sutera (1984) find that baroclinic instability and buoyancy conversion are substantial upon blocking, much greater than barotropic processes, but these processes are almost the same during nonblocking periods. Clearly, the processes similar in both the

Accepted for publication in *Journal of the Atmospheric Sciences*. DOI 10.1175/JAS-D-22-0220.1.

blocking and nonblocking (or climatology) can hardly be attributed to the critical factors controlling the blocking dynamics. The differences between the blocking and nonblocking (or climatology) events are hence focused on in performing dynamical studies for atmospheric blockings (e.g., Hansen and Sutera 1984; Fournier 2003; Ma and Liang 2017). We will follow this fashion in this section, i.e., analyzing the deviations of the multiscale processes from their respective climatological averages. Blockings are found to have an equivalent barotropic structure (e.g., Mak 1991; Ma and Liang 2017; Nabizadeh et al. 2021). What's more, we find that the multiscale canonical KE transfer processes are most vigorous near the tropopause through the troposphere, and their spatial patterns are almost the same on different levels (not shown), consistent with that in Ma and Liang (2017). We have also confirmed that the patterns of energetics integrated from 1000-hPa through 200-hPa are almost the same with that at 250 hPa. For these reasons, in this section, we will only focus on the 250-hPa level near the tropopause. Discussing blocking dynamics on a single level is a well-accepted practice in many previous studies, such as Mcwilliams (1980), Shutts (1983), Illari (1984), Nakamura et al. (1997), Fournier (2005), Nakamura and Huang (2018), Luo et al. (2005; 2019a).

a. Blocking and basic-flow interactions

The wave-flow interaction underlying a blocking can be quantitatively investigated by examining the canonical KE transfer between the basic flow window and blocking scale window. As significant temporal variations in blocking energetics have been reported in previous studies (e.g., Kushnir 1987; Ma and Liang 2017), we show the canonical KE transfer for the whole composite lifecycle of the blocking (Figs. 2-4). From the evolution of the geopotential of the blocking (contours in Figs. 2-4), the blocking signal is westward retrograding in its lifetime, during which it gradually gets stronger until day 0 and then becomes weaker. The underlying KE transfer is in pace with the blocking signal, i.e., it also gets stronger until day 0 and then becomes weaker.

Spatially, a zonal dipole appears in the distributions of the basic flow-to-blocking canonical KE transfers for all the Pacific, Atlantic and Ural blockings. To be specific, the basic flow transfers KE to the blocking at the western half of the blocking, while gaining KE from the blocking at the eastern half. Though the patterns of the dipoles are similar, their strengths and locations differ, and hence may have different implications on the respective blocking dynamics. In general, the dipole is strongest over the Pacific and weakest over the

Accepted for publication in *Journal of the Atmospheric Sciences*. DOI 10.1175/JAS-D-22-0220.1.

Atlantic. An observation is that the negative part of the dipole at the eastern half of the blocking over the Atlantic is negligible. In this sense, Pacific blockings tend to feed larger scales, in comparison to the Atlantic blockings. This may be the reason why reverse energy paths are found during blockings over the Pacific and Atlantic in Fournier (2003), with regard to the three largest scales at the block "location". Please note that the blocking "location" in Fournier's work covers the whole hemisphere, half of the hemisphere and 1/4 hemisphere for the first, second and third largest scales, respectively. As a result, the "location" covers the whole region of our blocking here. At the blocking location, the third largest scale gains more energy while the first and second large scales gain less energy through cross-scale transfer processes, i.e., negative energy transfer anomalies for larger scales and positive energy transfer anomalies for smaller scales ---- a downscale transfer anomaly, for the Atlantic blockings. In contrast, there is an upscale transfer anomaly for the Pacific blockings --- the second and third largest scales lose more energy and the first largest scale gains more energy. This is consistent with what we have found above. In other words, the seemingly contradictory observations for the Atlantic and Pacific blockings for large scale wave interactions in the framework of wavelets is actually unified in a fully localized view here --- they have similar transfer anomaly dipoles and energy paths, and the only differences are in the strengths of the dipoles over different regions.

Hansen and Sutera (1984) identifies a significant increase in KE transfer from the mean flow to wave-number 3 signals during blocking in the average Fourier-type energetics in four Atlantic cases. The results here are consistent, as is shown by the much stronger positive transfer in the western part of the Atlantic blocking compared to the negative transfer in the east part. As we know, the Fourier-type wavenumber energetics have no localized information retained, due to the global nature of Fourier transform. It is hence impossible to identify the location where a transfer occurs. By using the MWT-based localized energetics analysis, we can clearly see that the transfer processes concentrate in the western half of the Atlantic blocking. Quite differently, Fournier (2003) finds a positive transfer from the mean flow to the waves both at the upstream and downstream of the Atlantic blocking. This discrepancy may arise from the multiresolution nature of wavelets, with relative coarse resolution for large scales. To be specific, the "downstream of the blocking" in Fournier (2003) covers 1/4 of the hemisphere and the transfer will include all the processes in this large region. Another possible reason is that Fournier (2003) averages the transfer processes

Accepted for publication in *Journal of the Atmospheric Sciences*. DOI 10.1175/JAS-D-22-0220.1.

during all the blocking days, which may eliminate the temporal variation, which is observed to exist during the blocking lifecycle.

For the Pacific blockings, Fournier (2003) find an inverse KE transfer anomaly from long waves to the mean flow at the blocking, but here we see a dipole instead, i.e., both forward and inverse KE transfers exist. Again, this may be due to the coarse resolution for large scales in orthonormal wavelet analysis. Investigating the details of the dipole for the Pacific blockings, we find that its meridional center is located at the middle of the high cell and low cell. This is different from its peer over the Atlantic and Ural Mountain, where the dipoles are almost encircled by the high cells. This observation implies that the high cell and low cell of the Pacific blockings are more dynamically coupled than their counterparts over the other two regions, which can partially explain why the low cell over the Pacific is stronger than others.

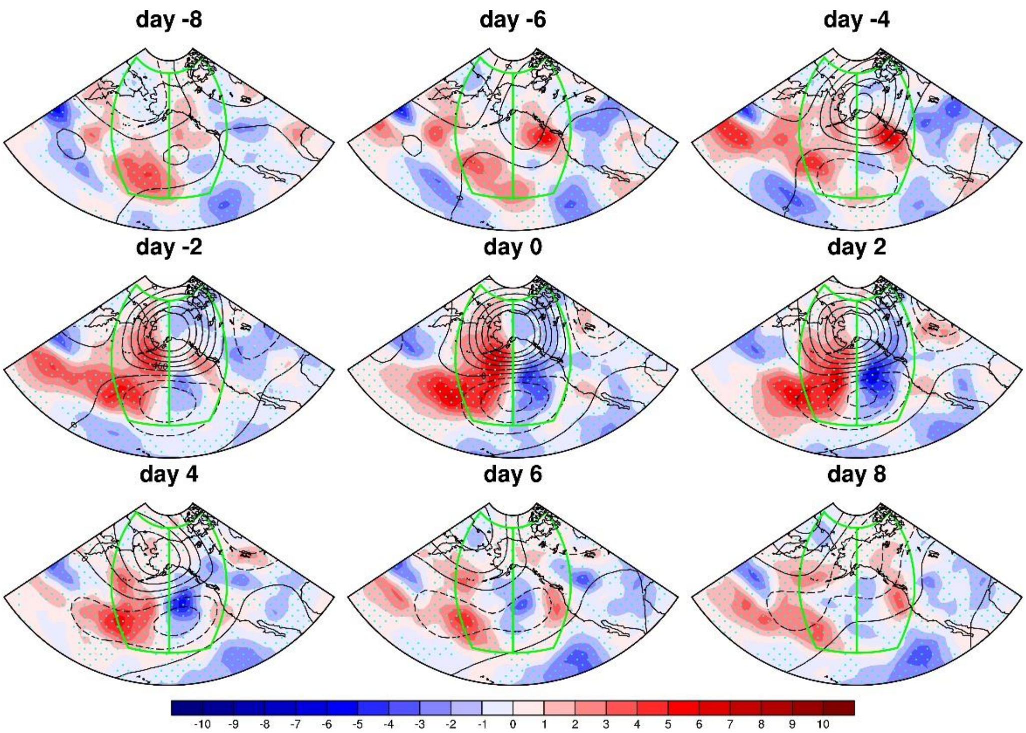

Fig. 2. KE transfer from the basic flow window to the blocking scale window ($\Gamma_K^{0\to1}$, in $10^{-4} m^2 s^{-3}$, shaded; same below) over the North Pacific Ocean at 250 hPa. Dotted are the regions of $\Gamma_K^{0\to1}$ statistically significant at the 99% level by the Student's t test. Green lines denote the regions where energetics in Figs. 8-9 are averaged.

Accepted for publication in *Journal of the Atmospheric Sciences*. DOI 10.1175/JAS-D-22-0220.1.

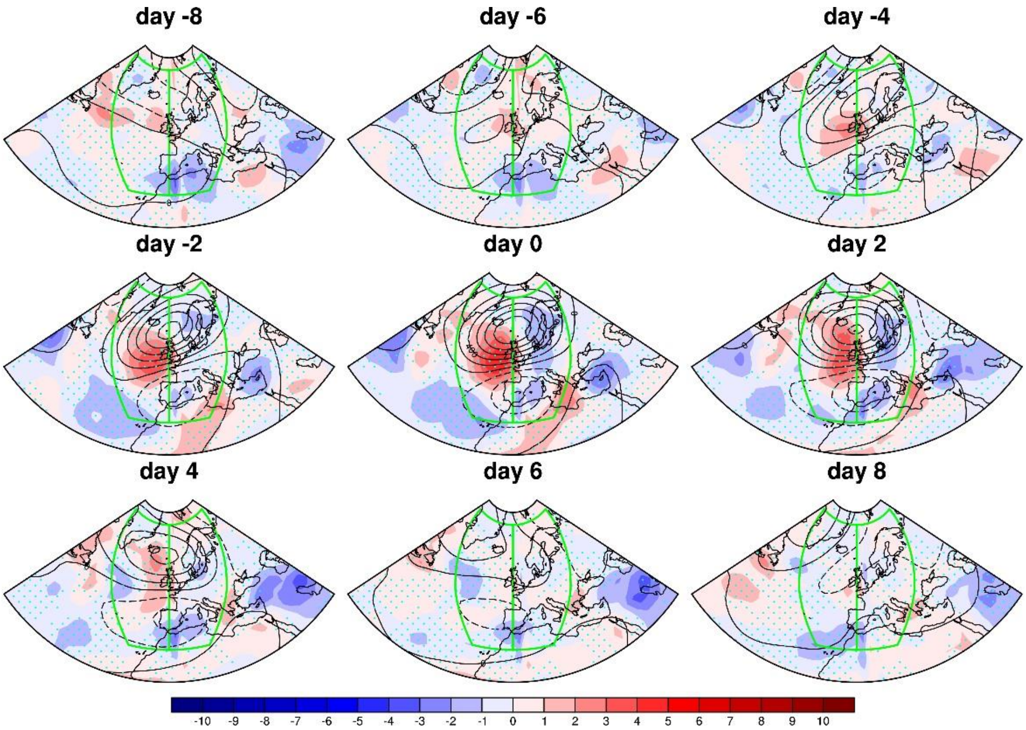

Fig. 3. KE transfer from the basic flow window to the blocking window ($\Gamma_K^{0\to1}$, in $10^{-4}m^2s^{-3}$, shaded; same below) over the North Atlantic Ocean at 250 hPa. Dotted are the regions of $\Gamma_K^{0\to1}$ statistically significant at the 99% level by the Student's t test. Green lines denote the regions where energetics in Figs. 8-9 are averaged.

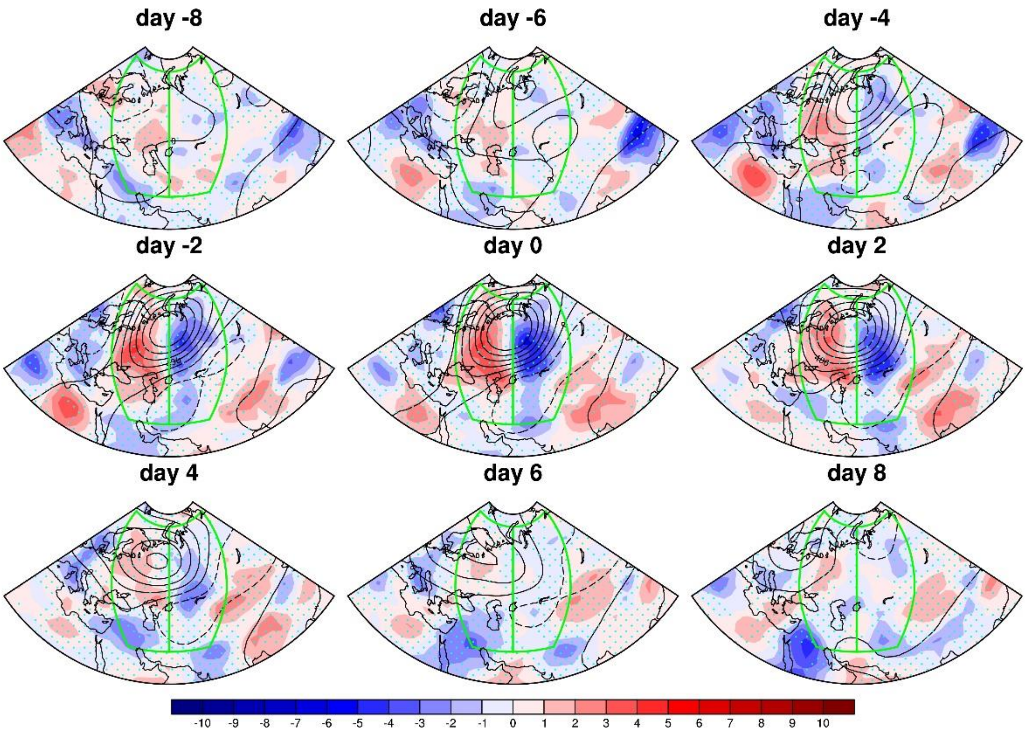

Fig. 4. KE transfer from the basic flow window to the blocking scale window ($\Gamma_K^{0\to1}$, in $10^{-4}m^2s^{-3}$, shaded; same below) over Ural Mountain at 250 hPa. Dotted are the regions of $\Gamma_K^{0\to1}$ statistically significant at the 99% level by the Student's t test. Green lines denote the

Accepted for publication in *Journal of the Atmospheric Sciences*. DOI 10.1175/JAS-D-22-0220.1.

regions where energetics in Figs. 8-9 are averaged.

b. Blocking-wave interactions

The canonical KE transfer from the high-frequency scale window to the blocking scale window is used to investigate the blocking-wave interactions. Generally, these interactions are characterized by an upscale KE transfer, i.e., a transfer from the high-frequency scale window to the blocking scale window (Figs. 5-7). This is consistent with most of the previous multiscale dynamical studies, both the theoretical studies (e.g., Shutts 1983; Luo et al. 2014) and energetics studies (e.g., Hansen and Chen 1982; Hansen and Sutera 1984; Fournier 2003; Ma and Liang 2017). The interactions, however, are spatially inhomogeneous, different from region to region. Over the Pacific and Ural Mountain, they exist at the eastern half of the respective blockings; in the Atlantic blocking, however, the interaction occurs at both western and eastern halves. This may account for the fact that, compared to other regions, Atlantic is mostly frequented by atmospheric blockings.

An intriguing new finding here is that the main upscale forcing of high-frequency exerts at the eastern half of the blocking, i.e., the downstream half of the blocking. It seems to be contradictory to the famous "eddy-straining mechanism" proposed by Shutts (1983), where it is claimed that the eddy forcing occurs at the upstream half of the blocking. Actually, previous studies have shown that eddy straining may not be the reason for the upscale forcing, but the result of downscale feedback from a developed blocking (Luo 2000, 2005; Luo et al. 2014). Possible mechanisms responsible for the downstream/upstream upscale forcing will be discussed later in Section 5.

We notice that Fournier (2003) comes up with a seemingly opposite conclusion regarding the upstream and downstream cascade underlying the Pacific blockings --- upscale/inverse transfer upstream while downscale/forward transfer downstream. However, the meaning of "upstream" and "downstream" is different from ours. As we all know, a wavelet spectrum has different resolutions for different scales. It is impossible to define "upstream" and "downstream" with respect to blocking center for larger scales in Fourier's work, since the "location" is larger than blocking---in fact it may cover the whole region of the blocking. As a result, the "upstream" and "downstream" are in a loose manner in Fourier's work. To be specific, the upstream and downstream for the Pacific blocking roughly refer to the regions west and east of the dateline (refer to Fourier's Fig. 14c). It is clear that Fournier's "downstream" includes both the upstream and our downstream here (cf.

Accepted for publication in *Journal of the Atmospheric Sciences*. DOI 10.1175/JAS-D-22-0220.1.

Fig. 2), while Fournier's "upstream" is much more westward than ours --- outside the Pacific blocking region here.. To be specific, the prominent downscale cascade for higher wavenumbers happens at locations 0, 2, 3 of the wavenumber band 5 in Fournier (2003). These locations cover the region $180 - 145^{\circ}W$ and the longitudinal centerline of his Pacific blockings is at nearly $138^{\circ}W$. As a result, his "downstream" is actually the western part of the blockings here, i.e. our upstream. Examining the energy cascade in the region, a slightly weak downscale cascade is also found here. In this sense, our findings here are not contradictory to Fournier's (2003).

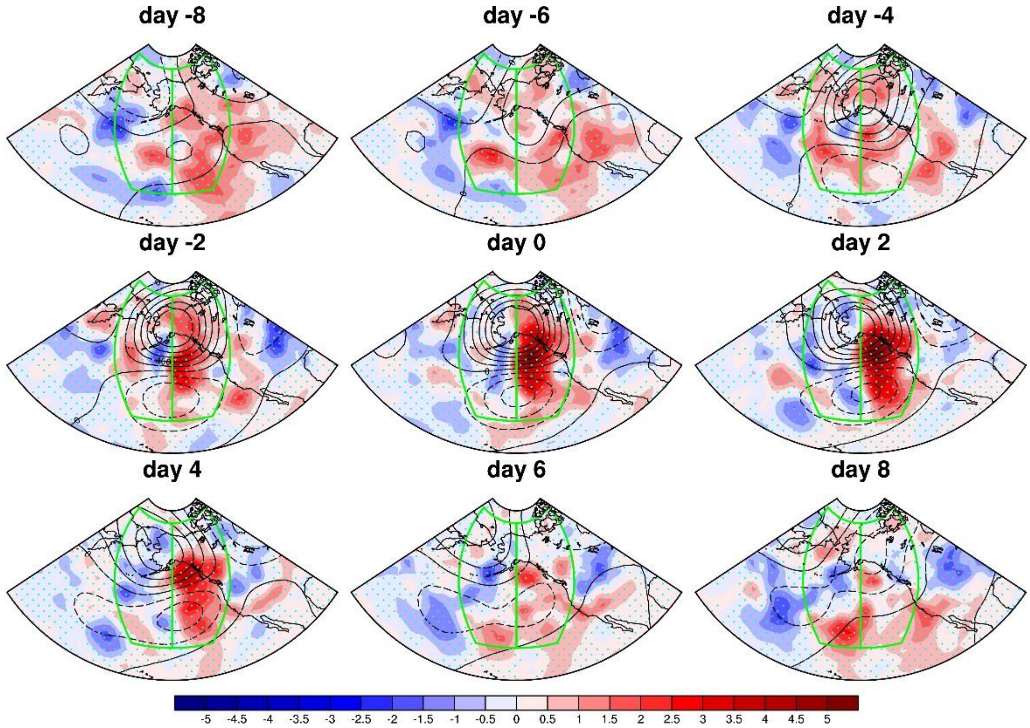

Fig. 5. KE transfer from the high frequency scale window to the blocking scale window ($\Gamma_K^{2\to1}$, in $10^{-4} m^2 s^{-3}$, shaded; same below) over the Pacific Ocean at 250 hPa. Dotted are the regions of $\Gamma_K^{2\to1}$statistically significant at the 99% level by the Student's t test. Green lines denote the regions where energetics in Figs. 8-9 are averaged.

File generated with AMS Word template 2.0

Accepted for publication in *Journal of the Atmospheric Sciences*. DOI 10.1175/JAS-D-22-0220.1.

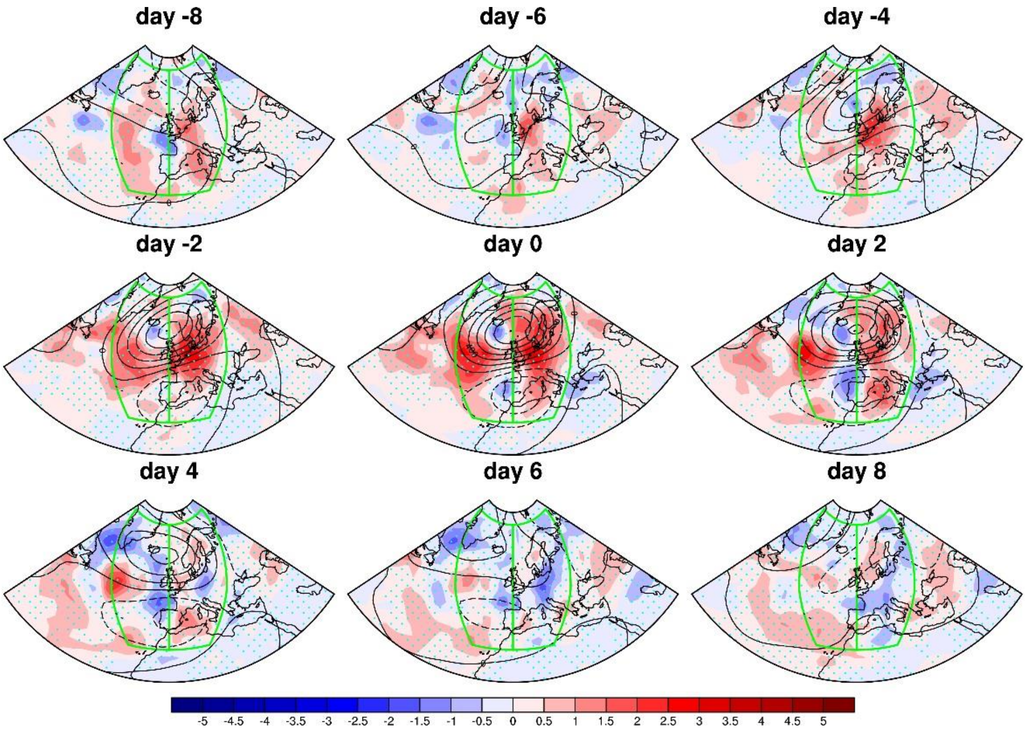

Fig. 6. KE transfer from the high frequency scale window to the blocking scale window ($\Gamma_K^{2\to1}$, in $10^{-4}m^2s^{-3}$, shaded; same below) over the North Atlantic Ocean at 250 hPa. Dotted are the regions of $\Gamma_K^{2\to1}$ statistically significant at the 99% level by the Student's t test. Green lines denote the regions where energetics in Figs. 8-9 are averaged.

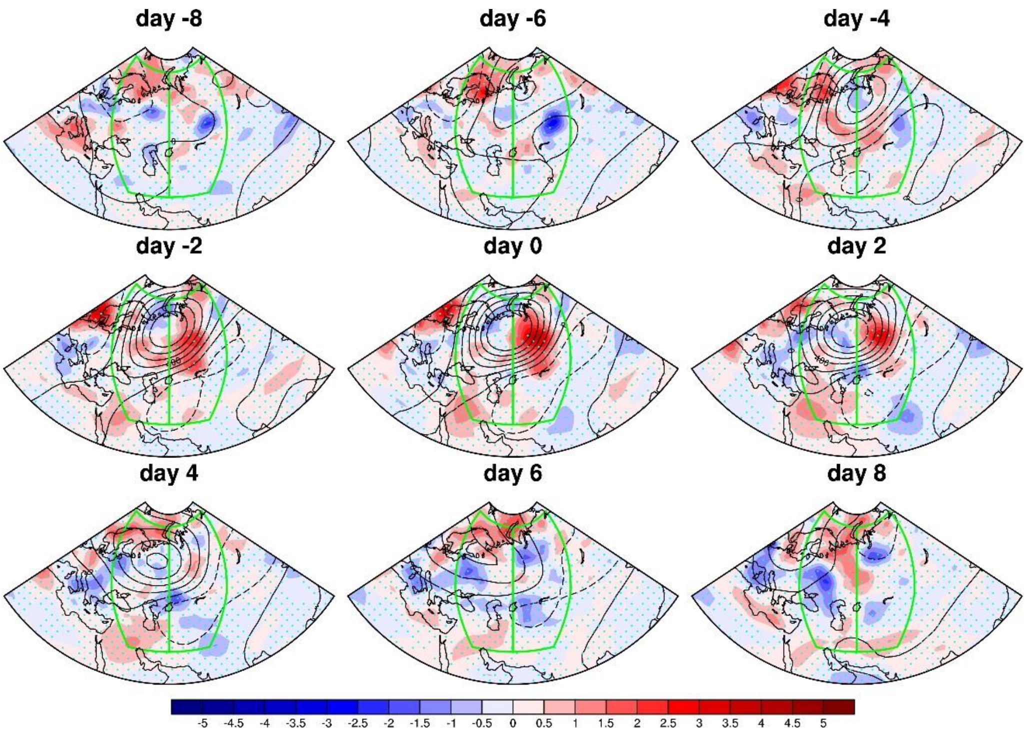

Fig. 7. KE transfer from the high frequency scale window to the blocking scale window ($\Gamma_K^{2\to1}$, in $10^{-4}m^2s^{-3}$, shaded; same below) over the Ural Mountain at 250 hPa. Dotted are the

Accepted for publication in *Journal of the Atmospheric Sciences*. DOI 10.1175/JAS-D-22-0220.1.

regions of $\Gamma_K^{2\to1}$ statistically significant at the 99% level by the Student's t test. Green lines denote the regions where energetics in Figs. 8-9 are averaged.

c. Upstream and downstream asymmetry of the KE cascade underlying the blockings

To further illustrate the upstream and downstream asymmetry, the time series of energetics averaged over the upstream and downstream (indicated by the green boxes in Figs. 2-7) during the blocking lifecycle are shown in Fig. 8. The asymmetry is clearly shown by distinct characteristics of the red (upstream) and blue (downstream) lines over all the three regions. From the blue lines, generally, in the downstream KE is transferred upscale from the high-frequency window to the blocking window, and from the blocking window to the basic flow. In contrast, the downscale cascade from the basic flow to the blocking is observed at the upstream of blockings. Different from the Pacific and Ural blockings, whose interactions with high-frequency window are really weak in upstream, the Atlantic blockings also experience a strong upscale forcing from the high-frequency window there. In a word, for all the Pacific, Atlantic and Ural Mountain blockings, there is a clear upscale cascade from the high-frequency to the basic flow via the blocking window at the downstream of the blockings, and a downscale cascade from the basic flow to the blockings at the upstream of blockings. The upscale cascade from the high-frequency window to the blocking window also happens, but only for the Atlantic blockings. In other words, the Atlantic blockings experience both upscale and downscale cascades at the upstream of the Atlantic blockings. Though the KE transfer from the high-frequency window to the blocking window in the upstream of the Pacific and Ural blockings is negligible compared to its downstream counterpart, it does contribute to blocking dynamics during a specific period ---- from day -8 to -2 (Figs. 8a and 8c). Thus it may be critical to the onset of Pacific and Ural blockings.

An overall observation is that magnitudes of all the energetics follow the pace of the blocking upon evolving. Luo et al. (2014) also propose, with the aid of an idealized model, that the eddy forcing to the blocking co-evolves with the blocking strength --- it intensifies when a blocking is strong and weakens when the blocking is weak. Our findings here are consistent with their theoretical works. However, by checking the details, we can find that there are subtle differences between the KE transfers over different regions. More specifically, the KE transfers from the high-frequency window and the basic flow to the blocking window in the downstreams of the Ural and Atlantic blockings attain their maxima on blocking day 0; but for the Pacific blocking, it is day 1 when the maximum is attained.

File generated with AMS Word template 2.0

Accepted for publication in *Journal of the Atmospheric Sciences*. DOI 10.1175/JAS-D-22-0220.1.

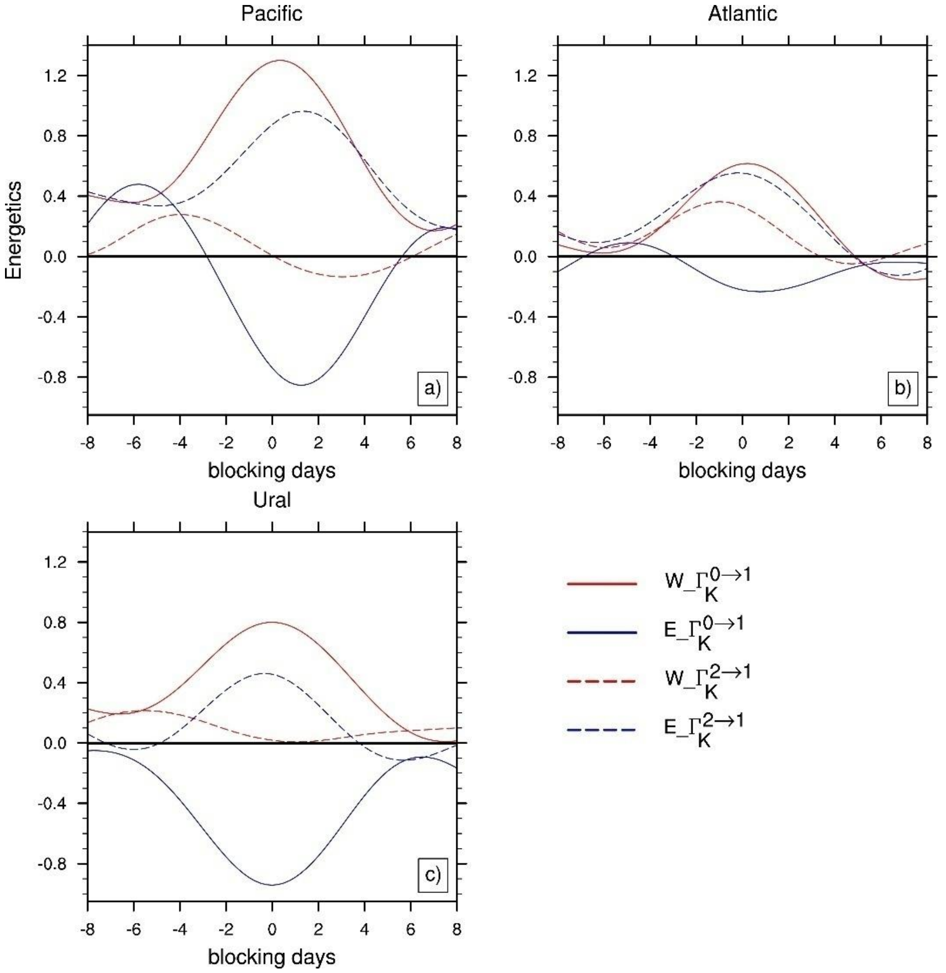

Fig. 8 Time series of energetics averaged over the upstream and downstream of blockings (the regions are illustrated by the green boxes in Figs. 2-7) from blocking day -8 to blocking day 8 over the Ural mountain, Atlantic and Pacific, respectively, including the upstream (W_$\Gamma_K^{2\to1}$, $in\ 10^{-4}m^2/s^3$) and downstream (E_$\Gamma_K^{2\to1}$, $in\ 10^{-4}m^2/s^3$) KE transfers from the high-frequency window to the blocking window, and the upstream (W_$\Gamma_K^{0\to1}$, $in\ 10^{-4}m^2/s^3$) and downstream (E_$\Gamma_K^{0\to1}$, $in\ 10^{-4}m^2/s^3$) KE transfers from the basic flow window to the blocking window. The bold black line is the abscissa.

To quantitatively compare the energetics over different regions, the time-mean energetics over the Ural Mountain, Atlantic and Pacific are shown in Fig. 9. The Pacific blocking has significantly stronger KE transfers both from the basic flow window and from the high-frequency window than the blockings over the two other regions. This is consistent with previous studies which find the cross-scale KE transfer underlying the Pacific blocking is

Accepted for publication in *Journal of the Atmospheric Sciences*. DOI 10.1175/JAS-D-22-0220.1.

more vigorous than that over the Atlantic (Hansen and Chen 1982; Hansen and Sutera 1984; Nakamura et al. 1997; Fournier 2003, 2005). For the Pacific and Ural blockings, though the upscale cascading from the high-frequency window to the blocking window are both positive over the upstream and downstream of the blockings, they are actually negligible over the respective upstream regions. While this confirms the essential role of the synoptic eddies to the blockings, to our best knowledge it, for the first time, tells their preference to the downstream of the blockings over the Pacific and Ural. In contrast, for the Atlantic blocking, the upscale forcing from the high-frequency processes to the blocking in the upstream is comparable with that in the downstream. Another observation is that the interaction between the blocking and the basic flow over the Atlantic is the weakest among the interactions over the three regions. The reason why there exists such a contrast among the three composite blockings is, probably, that the weak barotropic instability (positive canonical KE transfer) of the basic flow in the upstream of the Atlantic blocking cannot maintain the blocking; it can take effect only with the help from the synoptic eddies.

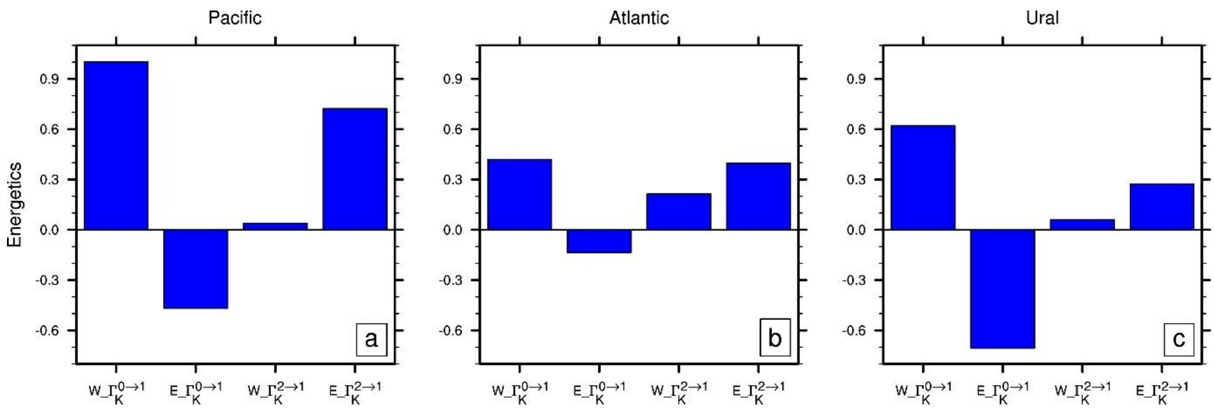

Fig. 9 Time-mean energetics, from blocking day -4 to blocking day 4, averaged over the upstream and downstream of the blockings (the regions are illustrated by the green boxes in Figs. 2-7), including the upstream ($W\_\Gamma_K^{2\to1}, in\ 10^{-4} m^2/s^3$) and downstream ($E\_\Gamma_K^{2\to1}, in\ 10^{-4} m^2/s^3$) KE transfers from the high-frequency window to the blocking window, and the upstream ($W\_\Gamma_K^{0\to1}, in\ 10^{-4} m^2/s^3$) and downstream ($E\_\Gamma_K^{0\to1}, in\ 10^{-4} m^2/s^3$) KE transfers from the basic flow window to the blocking window, respectively.

4. Discussion --- possible mechanisms underlying upscale forcing

Our outcomes seem to be inconsistent with some previous studies, such as and Illari (1984), Mullen (1987) and Nakamura et al. (1997), who find an "eddy forcing" one-quarter

Accepted for publication in *Journal of the Atmospheric Sciences*. DOI 10.1175/JAS-D-22-0220.1.

wavelength upstream the blocking. However, we don't think the outcomes of previous studies can be directly compared with ours. The different meanings of "eddy forcing" between theirs and ours may account for this inconsistency. The eddy forcing in Illari (1948), Mullen (1987) and Nakamura et al. (1997) is a quadratic term in the vorticity equation, while here we are talking about energetics, with the terms involving the products of three perturbation fields (c.f. Γ_K^{ϖ} in Eq. (4)). In this sense, it may be inappropriate that the canonical transfers here be compared to the previously discussed eddy forcings. Mak (1991) indeed investigates the eddy forcing to blocking from a multiscale energy perspective. But there are two issues in there which make his result different from ours. First, of course, the Reynolds decomposition as used is inappropriate for nonstationary signals, while our MWT is by design to tackle this kind of problem. The second, which is a more fundamental one, is that, even if Reynolds decomposition applies, canonical transfer is quite different from the interscale transfer in the classical formalism, which is adopted in Mak (1991). As long pointed out by, e.g., Holopainen (1978) and Plumb (1983), this classical empirical energetics formalism is problematic in that the separation of transfer from transport is not unique, and hence physically ambiguous. In a series of studies, Liang find that, besides this issue, another issue arises, which we elaborate a little bit hereafter (cf. Liang, 2016).

To demonstrate how a canonical transfer differs from its classical counterpart, consider the problem within the traditional Reynolds-decomposition framework so that a direct comparison can be made. Let T be a passive tracer which is placed in an incomporessible flow with velocity $\mathbf{v}$. The governing equation is hence

$$\frac{\partial T}{\partial t} + \nabla \cdot \left(\mathbf{v} T \right) = 0, \tag{6}$$

whose decomposed equations for the mean $\overline{T}$ and perturbation T' are, respectively,

$$\frac{\partial \overline{T}}{\partial t} + \nabla \cdot \left(\overline{\mathbf{v}}\overline{T} + \overline{\mathbf{v}'T'} \right) = 0, \tag{7}$$

$$\frac{\partial T'}{\partial t} + \nabla \cdot \left(\mathbf{v}'\overline{T} + \overline{\mathbf{v}}T' + \mathbf{v}'T' - \overline{\mathbf{v}'T'} \right) = 0. \tag{8}$$

Multiplying (7) by $\overline{T}$, and (8) by T', and taking the mean, one arrives at the evolutions of the mean energy and eddy energy.

File generated with AMS Word template 2.0

Accepted for publication in *Journal of the Atmospheric Sciences*. DOI 10.1175/JAS-D-22-0220.1.

$$\frac{\partial}{\partial t}\left(\frac{1}{2}\bar{T}^2\right)+\nabla\cdot\left(\frac{1}{2}\bar{\mathbf{v}}\bar{T}^2\right)=-\bar{T}\nabla\cdot\left(\overline{\mathbf{v}'T'}\right), \tag{9}$$

$$\frac{\partial}{\partial t}\left(\frac{1}{2}\overline{T'^2}\right)+\nabla\cdot\left(\frac{1}{2}\overline{\mathbf{v}T'^2}\right)=-\overline{\mathbf{v}'T'}\cdot\nabla\bar{T}. \tag{10}$$

The transfer term resulting from the above formalism, i.e., $\mathcal{R}\equiv-\overline{\mathbf{v}'T'}\cdot\nabla\bar{T}$ has been extensively utilized in meteorology for dynamic interpretation. However, it has long been found that this empirical transport-transfer separation is not unique and hence the resulting transfer seems to be ambiguous (Holopainen 1978, Plumb 1983). Moreover, Eqs. (9) and (10) do not, in general, sum to zero on the right hand side. This is not what one would expect of an energy transfer in the physical sense: An energy transfer should be, by physical intuition, a redistribution of energy among scale/scale windows, and in redistributing energy, the total energy must be conserved. Obviously the above violates the principle of energy conservation.

With the above MS-EVA formalism, these are not issues any more. As demonstrated in Liang (2016), the cross-scale energy transfer can be rigorously derived, and hence a unique separation of it from the multiscale transport is achieved naturally. In the case with a two-scale decomposition, and when the lowest scale level $j_0=0$ is chosen, plus a periodic extension, then the MWT is equivalent to the Reynolds decomposition (Liang & Anderson, 2007). In this special case, the equations corresponding to (9) and (10) become

$$\frac{\partial}{\partial t}\left(\frac{1}{2}\overline{T'^2}\right)+\nabla\cdot\left(\frac{1}{2}\overline{\mathbf{v}T'^2}+\frac{1}{2}\bar{T}\,\overline{\mathbf{v}'T'}\right)=\Gamma. \tag{11}$$

$$\frac{\partial}{\partial t}\left(\frac{1}{2}\bar{T}^2\right)+\nabla\cdot\left(\frac{1}{2}\bar{\mathbf{v}}\bar{T}^2+\frac{1}{2}\bar{T}\,\overline{\mathbf{v}'T'}\right)=-\Gamma, \tag{12}$$

where

$$\Gamma=\frac{1}{2}\left[\bar{T}\nabla\cdot\left(\overline{\mathbf{v}'T'}\right)-\overline{\mathbf{v}'T'}\cdot\nabla\bar{T}\right]. \tag{13}$$

Now one can see the right hand side is balanced: Eqs. (11) and (12) sum precisely to zero. Note this exact balance is not imposed; it is a natural corollary of the MWT-based formula as derived in Liang (2016). Also, as shown in Liang (2016), Γ has a Lie bracket form, reminiscent of the Poisson bracket in Hamiltonian dynamics. We hence call this Γ a

Accepted for publication in *Journal of the Atmospheric Sciences*. DOI 10.1175/JAS-D-22-0220.1.

“canonical transfer”. This rigorously derived formula has been validated in many benchmark problems, among which is the Kuo model for barotropic instability (Liang and Robinson, 2007).

For the problem in this study and for the purpose of comparison, consider a simple two-scale decomposition, i.e. $\mathbf{v} = \bar{\mathbf{v}} + \mathbf{v}'$. Here $\bar{\mathbf{v}}$ and $\mathbf{v}'$ represent velocity in blocking scale and high-frequency scale. To further simplify the problem, a basic flow ($\bar{u}$(y),0) is considered. Note that these assumptions are consistent with the real configuration of the blocking flow in the transition zone of the north high cell and south low cell over the Pacific and Atlantic, the very place where significant KE transfer occurs (the meridional velocity is nearly negligible) (Figs. 5-6). (For illustration purpose, we are not discussing the Ural case hereafter.) Under the above assumption, the canonical transfer term in Eq. (4) is reduced to (Liang and Robinson, 2007):

$$(1/2)\left[\bar{u}\nabla \cdot \overline{(\mathbf{v}'u')} - \overline{(u'v')}\partial\bar{u}/\partial y\right] \tag{14}$$

Note that the second term within the bracket is just the traditional Reynolds extraction. Here we have an extra term, and a prefactor 1/2. Note that the constant factor 1/2 just results in a difference in magnitude, not qualitative difference. So we just consider the terms within the bracket. Calculations (not shown) according to Eq. (14) show that the first term is dominant (2-3 times larger than the second term). This already tells why our result differs from those based on the classical formalism.

A closer look at the first term, i.e., $\bar{u}\nabla \cdot \overline{(\mathbf{v}'u')}$, reveals that it is a product of the background velocity and the divergence of negative Reynolds stress ($\overline{-(\mathbf{v}'u')}$) in the direction of u'. Recall that, in fluid mechanics, the divergence of a stress tensor means a force. Here it means the eddy force due to the Reynolds stress that *decelerates* $\bar{u}$, so the product of it with $\bar{u}$ means the work done by the eddy force in decelerating the basic flow. This does make sense, as it is the work decelerating the basic flow that makes the blocking grow.

By computation, the eddy forcing is most significant over the period from day -2 to 2 (Figs. 5-7). Hence, the distributions of $\overline{\mathbf{v}'u'}$ averaged over this period for the Pacific and Atlantic blockings are illustrated in Fig. 10. We know above that the divergence of this term is the eddy force that decelerates the basic flow, while by blocking it means the decelerating or obstructing of the basic flow. So the divergence of this term, i.e., the eddy forcing, tells where the blocking is fueled. From the figure it is clear that this kind of eddy forcing (i.e., the

Accepted for publication in *Journal of the Atmospheric Sciences*. DOI 10.1175/JAS-D-22-0220.1.

divergence of the streamlines) takes place in the downstream of the Pacific blockings, but both in the upstream and downstream of the Atlantic blockings. This is just as we have come up with by our MWT energetics analysis.

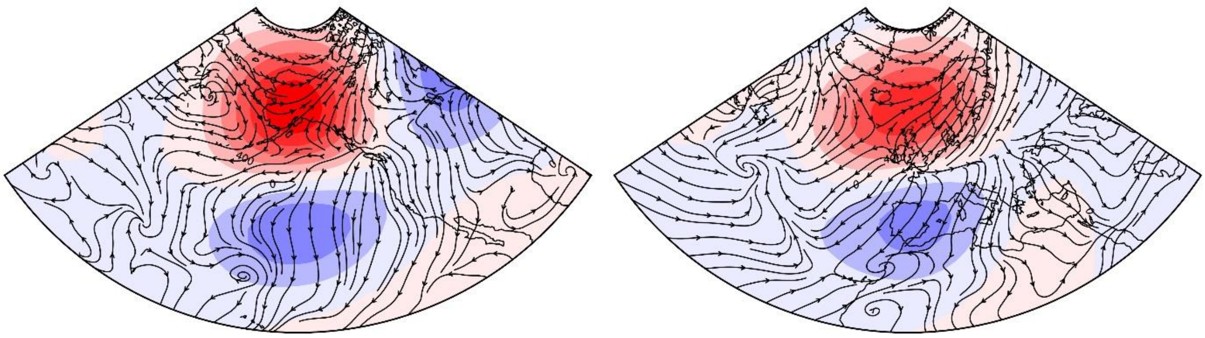

Fig. 10 Streamlines of $\mathbf{v}'u'$ averaged over blocking day -2 through day 2. The left (right) is for the Pacific (Atlantic) blocking. The shaded is the geopotential on the blocking window, which is used to denote the location of the blocking.

5. Energy budget

The above results clearly show that blocking dynamics differ in its upstream and downstream. It hence deserves an investigation of the local Lorenz energy cycles in the two regions separately. The results are shown in Figs. 11 and 12. The energetics are integrated from 1000hPa to 200hPa and averaged respectively over the upstream and downstream of blockings.

The canonical KE transfer from the basic flow window to the blocking window is the KE source and sink of the blockings in the upstream and downstream, respectively, for all the Pacific, Atlantic and Ural blockings. Upscale KE transfer from the high-frequency window forms a significant KE source of all the blockings in the downstream. It is also strong in the upstream of the Atlantic blocking but weak there for the Pacific and Ural blockings, consistent with the analysis above. KE is converted into APE in the downstream of all blockings through buoyancy conversion. However, its role varies with locations in the upstream. Specifically, positive buoyancy conversion from KE to APE occurs in the upstream of the Pacific blocking; negative one occurs there for the Ural blocking; and it is negligible there for the Atlantic blocking. Pressure work is found to vary with locations in both the upstream and downstream of the blockings. Positive pressure work occurs in the upstream of the Atlantic and Ural blockings, while negative one occurs there for the Pacific blocking.

Accepted for publication in *Journal of the Atmospheric Sciences*. DOI 10.1175/JAS-D-22-0220.1.

Negative pressure work takes effect in the downstream of the Pacific and Atlantic blockings, while it is positive there for the Ural blocking. The upstream and downstream are connected via KE transport from the former to the latter for all blockings. As a result, KE transport makes a KE sink for the upstream blockings while a KE source for the downstream blockings. In other words, the upstream part of the blockings contributes KE to their downstream part through transport process.

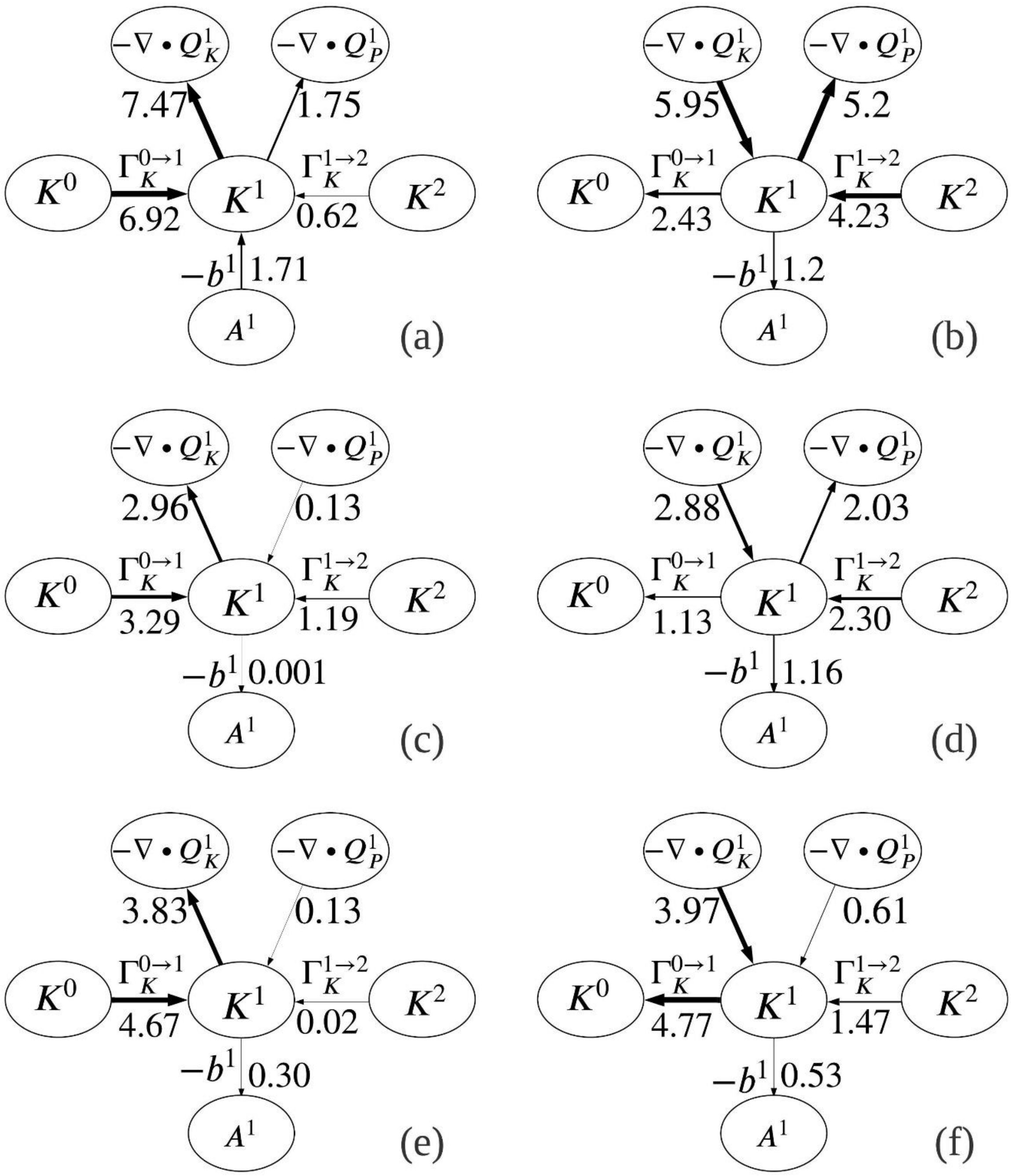

Accepted for publication in *Journal of the Atmospheric Sciences*. DOI 10.1175/JAS-D-22-0220.1.

Fig. 11. The KE energetics (in m^2/s^3) integrated through 1000hPa to 200hPa and averaged over the upstream (a, c, e) and downstream (b, d, f) regions of the Pacific (a, b), Atlantic (c, d), and Ural (e, f) blockings. The thickness of the arrows is proportional to the magnitude of the corresponding terms. The superscript 0, 1, and 2 represent the basic-flow, blocking and high-frequency windows, respectively. "K" and "A" stand for KE and APE; $\Gamma_K^{0\to1}$ and $\Gamma_K^{2\to1}$ are canonical KE transfers from the basic flow window and the high-frequency window to the blocking window, respectively; $-\nabla\cdot\mathbf{Q}_K^1$, $-\nabla\cdot\mathbf{Q}_P^1$ and $-b^1$ are KE transport, pressure work and buoyancy conversion from APE to KE on the blocking window.

On the APE budget, a unified Lorenz energy cycle is found in the downstream of all the blockings. To be specific, buoyancy conversion and canonical APE transfer from the basic flow to the blocking are sources, while APE transport and canonical APE transfer from the blocking window to the high-frequency window are sinks. In this cycle, a forward APE cascade is found, i.e., APE is transferred from the basic flow to the blocking window and then further downward to the high-frequency window. In the upstream, the APE cycles differ in location. For the Ural blocking, APE transport and buoyancy conversion are sources while APE transfers between the basic flow and the blocking window as well as that between the high-frequency window and the blockings window are sinks. For the Pacific blocking, the APE transfer from the basic flow to the blocking and APE transport on the blocking window are sources, while buoyancy conversion and APE transfer from the blocking window to the high-frequency window are sinks. For the Atlantic blocking, buoyancy conversion is negligible; APE transport is source and APE transfers among scales are sinks.

Accepted for publication in *Journal of the Atmospheric Sciences*. DOI 10.1175/JAS-D-22-0220.1.

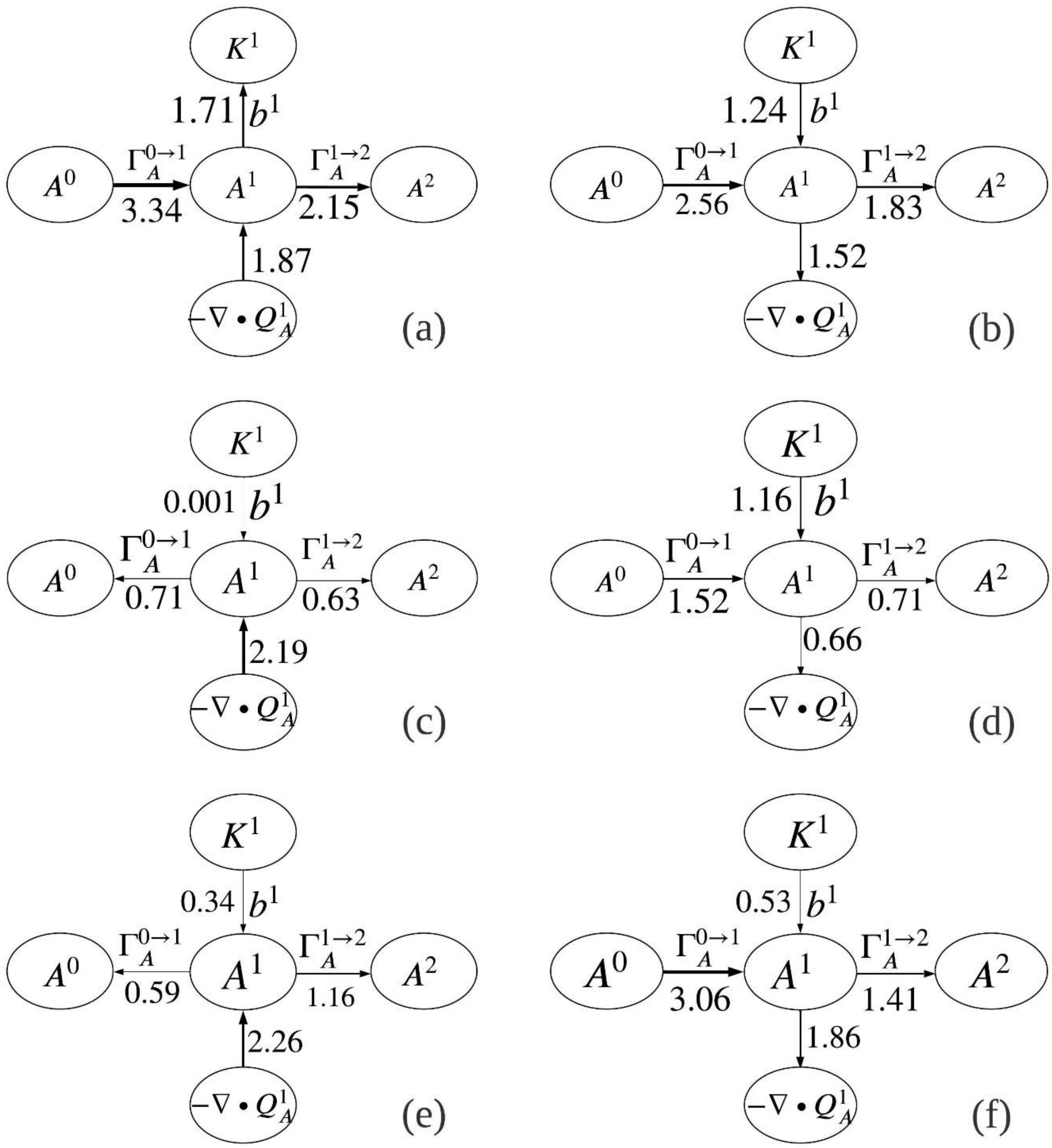

Fig. 12. As Fig. 11, but for the APE energetics (in m^2/s^3).

6. Summary and Conclusions

The multiscale interactions underlying the blockings over the Pacific, Atlantic and Ural Mountain have been investigated using the fully localized multiscale energetics analysis of Liang (2016), which is based on the functional analysis apparatus called multiscale window transform (Liang and Anderson, 2007) and the theory of canonical transfer (Liang, 2016). The four-dimensional field-like energetics allow for an accurate spatiotemporal pinpointing of the dynamical processes underlying the event of concern. The so-obtained results are

Accepted for publication in *Journal of the Atmospheric Sciences*. DOI 10.1175/JAS-D-22-0220.1.

generally consistent with previous studies, but also provide new insights to deepen the understanding of the blocking dynamics. The upscale forcing from the high-frequency storms, which have been discussed in many previous studies, has been confirmed here. However, the revealed locations of the forcings provide new information, which challenge the conclusion in some idealized theoretical works (e.g., Shutts, 1983). In contrast to the upscale forcing, the interaction between the basic flow and the blocking has been mostly overlooked. In this study, its role is investigated. Besides, the similarity and difference in the multiscale dynamics underlying the blockings over the three blocking-preferred regions, the Pacific, Atlantic and Ural Mountain, are also studied.

The blocking events are selected by well accepted criterion. Blocking day 0, or day 0 for brevity, is defined as the day when the blocking is strongest during its life cycle, and the days before and after day 0 are defined as days -1, -2, -3… and days 1, 2, 3…, respectively. Composition of variables related to a class of blockings for a particular day is accordingly performed by averaging these variables on the designated blocking day. To conduct multiscale interactions analysis, the original fields are firstly reconstructed onto three temporal scale windows using the multiscale window transform, namely, the basic flow window (above 64 days), the blocking window (16-64 days), and the high frequency window (less than 16 days). Clear blocking signals are observed in the composite blocking-scale geopotential, with a strong high cell at the north and a weak low cell at the south.

The interactions between the basic flow window and the blocking window are henceforth investigated with the methodology as mentioned above. A clear zonal dipolar structure is identified (Figs. 2-4), which has a positive canonical kinetic energy (KE) transfer at the western half of the blocking, and a negative KE transfer at the east. In other words, the blocking gains energy from the basic flow at upstream but loses energy to the basic flow at downstream. The quantitative nature of the analysis (Fig. 9) allows us to conclude that this process is critical to the blocking dynamics. At the upstream, the interaction between the blocking and the basic flow is much more important than the well-known upscale forcing from the synoptic storms. This result tells that the interaction between the basic flow and the blocking may have been overlooked. Though a unified dipolar pattern is found for all the blockings over the Pacific, Atlantic and Ural Mountain, their strengths differ. The positive KE transfer from the basic flow to the blocking at the upstream is the largest over the Pacific, and that over the Ural Mountain follows as the second; the weakest is that over the Atlantic

Accepted for publication in *Journal of the Atmospheric Sciences*. DOI 10.1175/JAS-D-22-0220.1.

(Fig. 9 and Figs. 2-4). Similarly, the negative KE transfer at the downstream is also the weakest (almost negligible) (Fig. 9 and Figs. 2-4) over the Atlantic; those over the Pacific and Ural Mountain are comparable.

The upscale forcing has been found in numerous blocking studies (e.g., Austin 1980; Illari and Marshall 1983; Tsou and Smith 1990; Robinson, 1991; Luo et al. 2014, 2019; Fournier 2003; Hansen and Chen 1982; Ma and Liang 2017; Nakamura and Huang 2018; Tanaka 1990; Martineau et al. 2022; Nakamura and Wallace 1993; Nakamura et al. 1997; Miller and Wang 2022). The results here confirm this conclusion. However, the downstream of the blocking is found to be the main location for the high-frequency processes to interact with the blocking. This finding implies a necessity to update the famous "eddy straining mechanism" (Shutts, 1983), in which the upscale forcing occurs at the upstream of the blocking. Nonetheless, we must emphasize that our results do not deny the eddy straining mechanism: while the upscale forcing from the high-frequency window to the blocking window is absent at the upstream of the Pacific and Ural Mountain blockings, it does exist at upstream of the Atlantic blocking. This finding here implies that the theory may need to be amended to allow for the downstream upscale forcing.

To conclude, for each of the three composite blockings, spatial asymmetry (mainly upstream-downstream asymmetry) has been identified on the maps of all the canonical KE transfers. In the downstream, observed is an inverse transfer from the high-frequency window all the way to the basic flow window, via the blocking window. In the upstream, significant interaction occurs only between the basic flow and the blocking, and the transfer is negligible between the synoptic eddies and the blocking over the Pacific and Ural Mountain. The Atlantic blocking is somewhat different: the interaction between the basic flow and the blocking is similar to its other peers; but an inverse cascading from the high-frequency window to the blocking window does find its way there, perhaps to collaborate with the relative weak Atlantic basic flow instability to maintain the blocking. These findings highlight the idiosyncrasy of the Atlantic blocking and the diversity in blocking dynamics.

Acknowledgments.

We are grateful to three anonymous referees, whose constructive advice helped improve the manuscript. This study is partially supported by National Natural Science Foundation of China under Grants 42005052, 41975064, and 42230105, by Southern Marine Science and

Accepted for publication in *Journal of the Atmospheric Sciences*. DOI 10.1175/JAS-D-22-0220.1.

Engineering Guangdong Laboratory (Zhuhai) through the Startup Foundation (#313022003, #313022005), by Shanghai B & R Joint Laboratory Project (#22230750300), and by Shanghai International Science and Technology Partnership Project (#21230780200). Part of the computational resources are provided by the NUIST High Performance Computing Center.

Data Availability Statement.

The ERA-40 datasets in this study are from https://apps.ecmwf.int/datasets/data/era40-daily/levtype=sfc/.

REFERENCES

Austin, J. F., 1980: The blocking of middle latitude westerly winds by planetary waves. *Q.J.R. Meteorol. Soc.*, **106**, 327–350, https://doi.org/10.1002/qj.49710644807.

Barnes, E. A., J. Slingo, and T. Woollings, 2011: A methodology for the comparison of blocking climatologies across indices, models and climate scenarios. *Clim Dyn*, **38**, 2467–2481, https://doi.org/10.1007/s00382-011-1243-6.

Barriopedro, D., R. García-Herrera, A. R. Lupo, and E. Hernández, 2006: A Climatology of Northern Hemisphere Blocking. *J. Climate*, **19**, 1042–1063, https://doi.org/10.1175/JCLI3678.1.

Dole, R., and Coauthors, 2011: Was there a basis for anticipating the 2010 Russian heat wave? *Geophysical Research Letters*, **38**, https://doi.org/10.1029/2010GL046582.

Dole, R. M., and N. D. Gordon, 1983: Persistent Anomalies of the Extratropical Northern Hemisphere Wintertime Circulation: Geographical Distribution and Regional Persistence Characteristics. *Monthly Weather Review*, **111**, 1567–1586, https://doi.org/10.1175/1520-0493(1983)111<1567:PAOTEN>2.0.CO;2.

Dong, L., C. Mitra, S. Greer, and E. Burt, 2018: The Dynamical Linkage of Atmospheric Blocking to Drought, Heatwave and Urban Heat Island in Southeastern US: A Multi-Scale Case Study. *Atmosphere*,.

Accepted for publication in *Journal of the Atmospheric Sciences*. DOI 10.1175/JAS-D-22-0220.1.

Drouard, M., and T. Woollings, 2018: Contrasting Mechanisms of Summer Blocking Over Western Eurasia. *Geophysical Research Letters*, **45**, 12,040-12,048, https://doi.org/10.1029/2018GL079894.

Fang, B., and M. Lu, 2020: Heatwave and Blocking in the Northeastern Asia: Occurrence, Variability, and Association. *Journal of Geophysical Research: Atmospheres*, **125**, e2019JD031627, https://doi.org/10.1029/2019JD031627.

Fournier, A., 2002: Atmospheric Energetics in the Wavelet Domain. Part I: Governing Equations and Interpretation for Idealized Flows. *J. Atmos. Sci.*, **59**, 1182–1197, https://doi.org/10.1175/1520-0469(2002)059<1182:AEITWD>2.0.CO;2.

——, 2003: Atmospheric Energetics in the Wavelet Domain. Part II: Time-Averaged Observed Atmospheric Blocking. *J. Atmos. Sci.*, **60**, 319–338, https://doi.org/10.1175/1520-0469(2003)060<0319:AEITWD>2.0.CO;2.

——, 2005: Instantaneous Wavelet Energetic Transfers between Atmospheric Blocking and Local Eddies. *J. Climate*, **18**, 2151–2171, https://doi.org/10.1175/JCLI3381.1.

Guo, Z., and X. S. Liang, 2022: Nexus of ambient flow and squall line via turbulence in the March 2018 meso-scale convective system over Southeast China. *Atmospheric Research*, **277**, 106287, https://doi.org/10.1016/j.atmosres.2022.106287.

Hansen, A. R., and T.-C. Chen, 1982: A Spectral Energetics Analysis of Atmospheric Blocking. *Mon. Wea. Rev.*, **110**, 1146–1165, https://doi.org/10.1175/1520-0493(1982)110<1146:ASEAOA>2.0.CO;2.

——, and A. Sutera, 1984: A comparison of the spectral energy and enstrophy budgets of blocking versus nonblocking periods. *Tellus A*, **36A**, 52–63, https://doi.org/10.1111/j.1600-0870.1984.tb00222.x.

Holopainen, E., 1978: *A Diagnostic study of the kinetic energy balance of the long-term mean flow and the associated transient fluctuations in the atmosphere*. University of Helsinki, Dept. of Meteorology,.

——, and C. Fortelius, 1987: High-Frequency Transient Eddies and Blocking. *J. Atmos. Sci.*, **44**, 1632–1645, https://doi.org/10.1175/1520-0469(1987)044<1632:HFTEAB>2.0.CO;2.

Accepted for publication in *Journal of the Atmospheric Sciences*. DOI 10.1175/JAS-D-22-0220.1.

Hong, C.-C., H.-H. Hsu, N.-H. Lin, and H. Chiu, 2011: Roles of European blocking and tropical-extratropical interaction in the 2010 Pakistan flooding. *Geophysical Research Letters*, **38**, https://doi.org/10.1029/2011GL047583.

Illari, L., 1984: A Diagnostic Study of the Potential Vorticity in a Warm Blocking Anticyclone. *J. Atmos. Sci.*, **41**, 3518–3526, https://doi.org/10.1175/1520-0469(1984)041<3518:ADSOTP>2.0.CO;2.

——, and J. C. Marshall, 1983: On the Interpretation of Eddy Fluxes During a Blocking Episode. *J. Atmos. Sci.*, **40**, 2232–2242, https://doi.org/10.1175/1520-0469(1983)040<2232:OTIOEF>2.0.CO;2.

Kautz, L.-A., O. Martius, S. Pfahl, J. G. Pinto, A. M. Ramos, P. M. Sousa, and T. Woollings, 2022: Atmospheric blocking and weather extremes over the Euro-Atlantic sector – a review. *Weather and Climate Dynamics*, **3**, 305–336, https://doi.org/10.5194/wcd-3-305-2022.

Kushnir, Y., 1987: Retrograding Wintertime Low-Frequency Disturbances over the North Pacific Ocean. *J. Atmos. Sci.*, **44**, 2727–2742, https://doi.org/10.1175/1520-0469(1987)044<2727:RWLFDO>2.0.CO;2.

Lejenäs, H., and H. Økland, 1983: Characteristics of northern hemisphere blocking as determined from a long time series of observational data. *Tellus A*, **35A**, 350–362, https://doi.org/10.1111/j.1600-0870.1983.tb00210.x.

Liang, X. S., 2016: Canonical Transfer and Multiscale Energetics for Primitive and Quasigeostrophic Atmospheres. *J. Atmos. Sci.*, **73**, 4439–4468, https://doi.org/10.1175/JAS-D-16-0131.1.

——, and A. R. Robinson, 2005: Localized multiscale energy and vorticity analysis: I. Fundamentals. *Dynamics of Atmospheres and Oceans*, **38**, 195–230, https://doi.org/10.1016/j.dynatmoce.2004.12.004.

——, and D. Anderson, 2007: Multiscale Window Transform. *Multiscale Model. Simul.*, **6**, 437–467, https://doi.org/10.1137/06066895X.

——, and A. R. Robinson, 2007: Localized multi-scale energy and vorticity analysis: II. Finite-amplitude instability theory and validation. *Dynamics of Atmospheres and Oceans*, **44**, 51–76, https://doi.org/10.1016/j.dynatmoce.2007.04.001.

File generated with AMS Word template 2.0

Accepted for publication in *Journal of the Atmospheric Sciences*. DOI 10.1175/JAS-D-22-0220.1.

Lorenz, E. N., 1955: Available Potential Energy and the Maintenance of the General Circulation. *Tellus*, **7**, 157–167, https://doi.org/10.1111/j.2153-3490.1955.tb01148.x.

Luo, B., D. Luo, A. Dai, I. Simmonds, and L. Wu, 2021: A Connection of Winter Eurasian Cold Anomaly to the Modulation of Ural Blocking by ENSO. *Geophysical Research Letters*, **48**, e2021GL094304, https://doi.org/10.1029/2021GL094304.

Luo, D., 2000: Planetary-scale baroclinic envelope Rossby solitons in a two-layer model and their interaction with synoptic-scale eddies. *Dynamics of Atmospheres and Oceans*, **32**, 27–74, https://doi.org/10.1016/S0377-0265(99)00018-4.

——, 2005: A Barotropic Envelope Rossby Soliton Model for Block–Eddy Interaction. Part I: Effect of Topography. *J. Atmos. Sci.*, **62**, 5–21, https://doi.org/10.1175/1186.1.

——, J. Cha, L. Zhong, and A. Dai, 2014: A nonlinear multiscale interaction model for atmospheric blocking: The eddy-blocking matching mechanism. *Q.J.R. Meteorol. Soc.*, **140**, 1785–1808, https://doi.org/10.1002/qj.2337.

——, Y. Xiao, Y. Diao, A. Dai, C. L. E. Franzke, and I. Simmonds, 2016: Impact of Ural Blocking on Winter Warm Arctic–Cold Eurasian Anomalies. Part II: The Link to the North Atlantic Oscillation. *Journal of Climate*, **29**, 3949–3971, https://doi.org/10.1175/JCLI-D-15-0612.1.

——, X. Chen, J. Overland, I. Simmonds, Y. Wu, and P. Zhang, 2019a: Weakened Potential Vorticity Barrier Linked to Recent Winter Arctic Sea Ice Loss and Midlatitude Cold Extremes. *J. Climate*, **32**, 4235–4261, https://doi.org/10.1175/JCLI-D-18-0449.1.

——, W. Zhang, L. Zhong, and A. Dai, 2019b: A Nonlinear Theory of Atmospheric Blocking: A Potential Vorticity Gradient View. *J. Atmos. Sci.*, **76**, 2399–2427, https://doi.org/10.1175/JAS-D-18-0324.1.

Ma, J., and X. S. Liang, 2017: Multiscale Dynamical Processes Underlying the Wintertime Atlantic Blockings. *J. Atmos. Sci.*, **74**, 3815–3831, https://doi.org/10.1175/JAS-D-16-0295.1.

Mak, M., 1991: Dynamics of an atmospheric blocking as deduced from its local energetics. *Quarterly Journal of the Royal Meteorological Society*, **117**, 477–493, https://doi.org/10.1002/qj.49711749904.

Accepted for publication in *Journal of the Atmospheric Sciences*. DOI 10.1175/JAS-D-22-0220.1.

Martineau, P., H. Nakamura, A. Yamamoto, and Y. Kosaka, 2022: Baroclinic Blocking. *Geophysical Research Letters*, **49**, e2022GL097791, https://doi.org/10.1029/2022GL097791.

McWilliams, J. C., 1980: An application of equivalent modons to atmospheric blocking. *Dynamics of Atmospheres and Oceans*, **5**, 43–66, https://doi.org/10.1016/0377-0265(80)90010-X.

Miller, D. E., and Z. Wang, 2022: Northern Hemisphere Winter Blocking: Differing Onset Mechanisms across Regions. *Journal of the Atmospheric Sciences*, **79**, 1291–1309, https://doi.org/10.1175/JAS-D-21-0104.1.

Miller, R. L., G. M. Lackmann, and W. A. Robinson, 2020: A New Variable-Threshold Persistent Anomaly Index: Northern Hemisphere Anomalies in the ERA-Interim Reanalysis. *Monthly Weather Review*, **148**, 43–62, https://doi.org/10.1175/MWR-D-19-0144.1.

Mullen, S. L., 1987: Transient Eddy Forcing of Blocking Flows. *J. Atmos. Sci.*, **44**, 3–22, https://doi.org/10.1175/1520-0469(1987)044<0003:TEFOBF>2.0.CO;2.

Nabizadeh, E., S. W. Lubis, and P. Hassanzadeh, 2021: The 3D Structure of Northern Hemisphere Blocking Events: Climatology, Role of Moisture, and Response to Climate Change. *Journal of Climate*, **34**, 9837–9860, https://doi.org/10.1175/JCLI-D-21-0141.1.

Nakamura, H., and J. M. Wallace, 1993: Synoptic Behavior of Baroclinic Eddies during the Blocking Onset. *Mon. Wea. Rev.*, **121**, 1892–1903, https://doi.org/10.1175/1520-0493(1993)121<1892:SBOBED>2.0.CO;2.

——, M. Nakamura, and J. L. Anderson, 1997: The Role of High- and Low-Frequency Dynamics in Blocking Formation. *Mon. Wea. Rev.*, **125**, 2074–2093, https://doi.org/10.1175/1520-0493(1997)125<2074:TROHAL>2.0.CO;2.

Nakamura, N., and C. S. Y. Huang, 2018: Atmospheric blocking as a traffic jam in the jet stream. *Science*, **361**, 42–47, https://doi.org/10.1126/science.aat0721.

Pelly, J. L., and B. J. Hoskins, 2003: A New Perspective on Blocking. *J. Atmos. Sci.*, **60**, 743–755, https://doi.org/10.1175/1520-0469(2003)060<0743:ANPOB>2.0.CO;2.

Plumb, R. A., 1983: A New Look at the Energy Cycle. *J. Atmos. Sci.*, **40**, 1669–1688, https://doi.org/10.1175/1520-0469(1983)040<1669:ANLATE>2.0.CO;2.

File generated with AMS Word template 2.0

Accepted for publication in *Journal of the Atmospheric Sciences*. DOI 10.1175/JAS-D-22-0220.1.

Robinson, W. A., 1991: The Dynamics of Low-Frequency Variability in a Simple Model of the Global Atmosphere. *J. Atmos. Sci.*, **48**, 429–441, https://doi.org/10.1175/1520-0469(1991)048<0429:TDOLFV>2.0.CO;2.

Sawyer, J. S., 1970: Observational characteristics of atmospheric fluctuations with a time scale of a month. *Q.J.R. Meteorol. Soc.*, **96**, 610–625, https://doi.org/10.1002/qj.49709641005.

Shutts, G. J., 1983: The propagation of eddies in diffluent jetstreams: Eddy vorticity forcing of ‘blocking’ flow fields. *Q.J.R. Meteorol. Soc.*, **109**, 737–761, https://doi.org/10.1002/qj.49710946204.

Song, K., L. Tao, and Y. Yang, 2022: On the intensification of typhoon Damrey with the monsoon gyre. *Quarterly Journal of the Royal Meteorological Society*, **n/a**, https://doi.org/10.1002/qj.4425.

Tanaka, H. L., 1990: A Numerical Simulation of Amplification of Low-Frequency Planetary Waves and Blocking Formations by the Upscale Energy Cascade. *Mon. Wea. Rev.*, **119**, 2919–2935, https://doi.org/10.1175/1520-0493(1991)119<2919:ANSOAO>2.0.CO;2.

Tibaldi, S., and F. Molteni, 1990: On the operational predictability of blocking. *Tellus A*, **42**, 343–365, https://doi.org/10.1034/j.1600-0870.1990.t01-2-00003.x.

Trigo, R. M., I. F. Trigo, C. C. DaCamara, and T. J. Osborn, 2004: Climate impact of the European winter blocking episodes from the NCEP/NCAR Reanalyses. *Climate Dynamics*, **23**, 17–28, https://doi.org/10.1007/s00382-004-0410-4.

Tsou, C.-H., and P. J. Smith, 1990: The role of synoptic/planetary–scale interactions during the development of a blocking anticyclone. *Tellus A*, **42**, 174–193, https://doi.org/10.1034/j.1600-0870.1990.00015.x.

Uppala, S. M., and Coauthors, 2005: The ERA-40 re-analysis. *Q.J.R. Meteorol. Soc.*, **131**, 2961–3012, https://doi.org/10.1256/qj.04.176.

Xu, F., and X. S. Liang, 2020: The Synchronization between the Zonal Jet Stream and Temperature Anomalies Leads to an Extremely Freezing North America in January 2019. *Geophysical Research Letters*, **47**, e2020GL089689, https://doi.org/10.1029/2020GL089689.

Accepted for publication in *Journal of the Atmospheric Sciences*. DOI 10.1175/JAS-D-22-0220.1.

Yang, Y., R. H. Weisberg, Y. Liu, and X. San Liang, 2020: Instabilities and Multiscale Interactions Underlying the Loop Current Eddy Shedding in the Gulf of Mexico. *J. Phys. Oceanogr.*, **50**, 1289–1317, https://doi.org/10.1175/JPO-D-19-0202.1.

——, J. C. McWilliams, X. San Liang, H. Zhang, R. H. Weisberg, Y. Liu, and D. Menemenlis, 2021: Spatial and Temporal Characteristics of the Submesoscale Energetics in the Gulf of Mexico. *Journal of Physical Oceanography*, **51**, 475–489, https://doi.org/10.1175/JPO-D-20-0247.1.

Zhao, Y.-B., X. S. Liang, Z. Guan, and K. I. Hodges, 2019: The asymmetric eddy–background flow interaction in the North Pacific storm track. *Quarterly Journal of the Royal Meteorological Society*, **145**, 575–596, https://doi.org/10.1002/qj.3453.

Accepted for publication in *Journal of the Atmospheric Sciences*. DOI 10.1175/JAS-D-22-0220.1.